Article

Not peer-reviewed version

Photonic Vacuum Windows: A Casimir-Safe Operational Baseline

André J. H. Kamminga *

Posted Date: 6 November 2025

doi: 10.20944/preprints202511.0290.v1

Keywords: unification; field theory; bounded vacuum; emergence; analytic consistency; reference frame

Article

Photonic Vacuum Windows: A Casimir-Safe Operational Baseline

André J. H. Kamminga

Independent researcher, The Netherlands; a.kamminga@ziggo.nl

Abstract

We propose a physical picture in which light propagation in vacuum is carried by a sea of fluctuating degrees of freedom. At the effective, linear-response scale, this collective medium determines the electromagnetic properties that govern how light moves, while preserving the characteristic impedance of the vacuum and avoiding artefacts arising from arbitrary parameter choices. This conceptual idea forms the primary aim of this work. To test whether this picture is realistic, we propose a platform-independent and testable approach. We introduce a simple band-averaged reporting measure that reduces any measurement to a single comparable quantity derived from the spectral weighting of the experiment. Using first-order, model-independent relations, we show how this quantity connects to observable shifts in cavity frequencies, interferometric phase, radiometric balance, and Casimir measurements. These links are presented solely as consequences that render the concept empirically testable, not as applications in themselves. The approach is constrained by the standard principles of linear response, causality, passivity, and a high-frequency limit consistent with Maxwell electrodynamics, so that the carried-light picture remains compatible with established physics and testable through reproducible, band-averaged limits on deviations from ideal vacuum propagation.

Keywords: unification; field theory; bounded vacuum; emergence; analytic consistency; reference frame

---

1. Introduction

Our aim is *conceptual*; empirical links serve solely to make the concept falsifiable.
Classical electrodynamics treats free space as a linear, dispersionless background with fixed electromagnetic parameters and a universal light speed [12,19]. From a quantum perspective, however, the vacuum is an active ground state whose fluctuations give rise to observable phenomena, notably the Casimir effect and radiative corrections [2–4,8,10,13,16,20,25,26]. Taking that perspective seriously, we advance a *carried-light* picture: electromagnetic waves propagate through—and are effectively carried by—a sea of fluctuating degrees of freedom whose collective response sets how light moves.

Note: These mappings are presented only as *testable consequences*. The primary contribution is a **conceptual, impedance-invariant, and physically admissible** description of the carried-light vacuum.

Primary Aim

The aim of this work is conceptual: to articulate a physically admissible, testable description in which the collective vacuum fluctuations determine the effective electromagnetic response while preserving the vacuum impedance. The experimental mappings (cavities, interferometers, radiometry, and Casimir) are presented only as *consequences* that enable empirical tests of the concept, not as applications in themselves.

Relation to Prior Work

This formulation extends the author's earlier studies on an energetically bounded quantum vacuum, which proposed a finite, self-consistent fluctuation ensemble co-determining the observed

 doi:10.20944/preprints202511.0290.v1

light speed and quantum behaviour [14,15]. Related ideas also link the speed of light to vacuum fluctuations [37], typically without an explicit energetic bound. Here that bound acts as a natural physical regularisation: it ensures a finite energy density and motivates an operational, Casimir-safe framework directly testable in the laboratory.

Operationalisation

To make the idea testable without committing to a microscopic model, we adopt a single, frequency-dependent vacuum response (a "window") that captures small, causal and passive departures from ideal propagation while keeping the free-space impedance fixed. Any measurement is paired with a calibrated, unit-area sensitivity curve from the relevant platform, yielding a band-averaged figure that collapses apparatus specifics into a published sensitivity window. Publishing this figure alongside the window enables like-for-like comparison and reanalysis across precision photonic platforms [1,5,9,31,35].

Light as Reference and Messenger

Within this approach, light plays a dual role. It provides the practical reference for distance, time and causality, and it acts as the primary information carrier whose bandwidth, noise floor and dispersion are constrained by the vacuum response. Small departures from ideal behaviour are therefore naturally expressed as band-averaged deformations of that response and confronted with photonic observations, including broadband radiometry and astrophysical calibrations [11,21,29].

Physical Admissibility

The vacuum window is required to satisfy standard linear-response principles that underpin fluctuation–dissipation reasoning: causality (Kramers–Kronig consistency), passivity (non-negative dissipation), and a high-frequency limit consistent with Maxwell electrodynamics [6,12,17–19]. These conditions ensure compatibility with established physics and with precision constraints from Casimir and optical experiments [4,16,26] while allowing tiny, KK-consistent dispersive features to be probed.

Scope and Contributions

In summary, this paper (i) motivates the carried-light view of an energetically bounded vacuum; (ii) formulates a Casimir-safe, impedance-invariant operational window; (iii) provides first-order, platform-agnostic mappings to cavity frequency shifts, interferometric phase, group delay, conservative radiometric propagation, and Casimir-type observables; and (iv) outlines reporting conventions that enable cross-platform synthesis via a band-averaged figure and the published sensitivity. The reporting approach aligns with current best practices in open and reproducible research [27,28,34,36]. The result is a practical route to measurement that remains faithful to the conceptual picture while enabling reproducible constraints on deviations from ideal vacuum propagation.

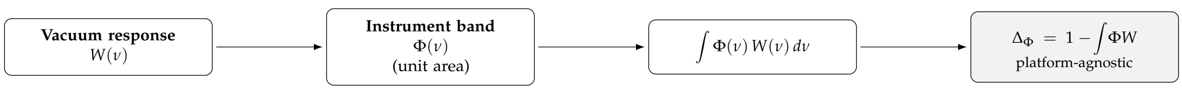

Figure 1. Operational pipeline: a single vacuum window $W(\nu)$ and a calibrated, unit-area sensitivity $\Phi(\nu)$ combine into the platform-independent figure of merit Δ_Φ.
Normalization: $\int \Phi(\nu)\, d\nu = 1$ (unit-area). Curves rescaled for visibility; schematic, not to scale.

What follows is an operational interface for falsifiability, not an application program.

Motivation and Scope

The perspective of an *energetically bounded quantum vacuum* provides a natural physical motivation for introducing a controlled, measurable deformation of the vacuum response. In this picture, the electromagnetic vacuum is not perfectly featureless but possesses a finite, self-consistent energy density that limits the extent of quantum fluctuations [14,15]. The constancy of the observed speed of light

doi:10.20944/preprints202511.0290.v1

then arises as an emergent equilibrium property of this bounded fluctuation ensemble, consistent with theoretical arguments that link the light speed to the structure of the quantum vacuum [37]. Small residual departures from this equilibrium can, in principle, be probed as frequency-dependent variations in the effective vacuum response.

Directly testing such effects requires an operational formulation that is independent of the detailed microscopic model yet compatible with known physical constraints. We therefore seek a framework that:

- preserves electromagnetic impedance invariance, ensuring no artificial boundary reflections arise from the parametrisation itself;
- remains consistent with passivity and Kramers-Kronig relations, guaranteeing a physically admissible (causal and dissipative) response;
- smoothly approaches the classical limit at high frequencies where experimental bounds are already tight;
- allows results from distinct photonic platforms—cavities, interferometers, radiometric propagation, and Casimir experiments—to be reported in a common metric.

The *vacuum window* $W(\nu)$ proposed here satisfies these requirements. It represents the collective electromagnetic response of the bounded vacuum while maintaining a fixed impedance. Its corresponding *band figure of merit*, Δ_Φ, constructed from a measured instrument sensitivity function $\Phi(\nu)$, provides a single, reproducible number that quantifies any observed deviation from the ideal vacuum. Publishing both $\Phi(\nu)$ and Δ_Φ enables direct, cross-platform comparison and reanalysis.

This approach does not attempt to describe the microscopic origin of the bounded-vacuum structure; instead, it offers a phenomenologically faithful and experimentally transparent interface between that theoretical picture and measurable observables. In this sense, the present work forms a bridge between the conceptual framework of an energetically bounded quantum vacuum and the quantitative methodologies of modern precision photonics.

Having established the physical motivation and constraints that guide the formulation, we now develop the explicit impedance-invariant window framework that operationalises these ideas. This section introduces the mathematical form of the vacuum window, its connection to measurable observables, and the consistency conditions that ensure physical admissibility and Casimir-safety across frequency domains.

2. Operational Interface for Falsifiability

The role of $W(\nu)$, $\Phi(\nu)$, and Δ_Φ is purely operational: to render the conceptual proposal empirically testable and reportable.

$\Delta_\Phi \equiv 1 - \int \Phi(\nu)\, W(\nu)\, d\nu$, $W = 1 + \delta W$. **Sign:** $+\delta W$ denotes effective slowdown. Isotropic SME: $n - 1 = -\bar{\kappa}_{\rm tr} \Rightarrow \delta W = -\bar{\kappa}_{\rm tr}$.

We model the vacuum as linear, isotropic and homogeneous with a single scalar response ("window") $W(\nu)$ that co-scales the electromagnetic parameters while preserving the wave impedance:

$$\varepsilon(\nu) = \varepsilon_0\, W(\nu), \qquad \mu(\nu) = \mu_0\, W(\nu), \tag{1}$$

so that $Z(\nu) = \sqrt{\mu(\nu)/\varepsilon(\nu)} = Z_0$ remains constant and no spurious boundary-impedance effects are introduced [12,19].

We adopt the **notation convention**

$$n(\nu) = W(\nu), \qquad c_{\rm eff}(\nu) = \frac{c}{W(\nu)}, \tag{2}$$

and use it consistently throughout (this removes common factor/sign ambiguities in mappings to observables and SME parameters).

Preprints.org (www.preprints.org) | NOT PEER-REVIEWED | Posted: 6 November 2025 doi:10.20944/preprints202511.0290.v1

Operational response factor and free-space reference. The proposed frequency-dependent response factor $W(\nu)$ makes the concept of a fluctuating quantum vacuum operational. It represents the collective influence of all virtual fluctuations without modelling their microscopic details individually, thus describing how the vacuum behaves as an effective medium for electromagnetic propagation.

The construction of $W(\nu)$ follows three fundamental requirements:

- **Causality** — the response to an electromagnetic excitation must occur only after the stimulus itself; in the frequency domain this leads to the Kramers-Kronig relations linking the real and imaginary parts of $W(\nu)$.
- **Passivity** — the vacuum cannot generate energy, only store or dissipate it; mathematically, $\operatorname{Im} W(\nu) \geq 0$ for positive frequencies.
- **Free-space limit** — at very high frequencies ($\nu \to \infty$) the influence of the fluctuating background vanishes and $W(\nu)$ approaches unity. This limit represents the ideal *free-space* of classical Maxwell theory: homogeneous, lossless, and dispersionless, where light propagates with constant speed c.

Free-space thus acts as a *reference state*: it defines the zero-deviation baseline against which the frequency-dependent properties of the real, fluctuating vacuum are measured. Whenever $W(\nu) \neq 1$, light propagation is no longer perfectly ideal. Such deviations imply that the quantum vacuum itself—as a medium—subtly influences the speed, phase, and group structure of electromagnetic waves. In this sense, light does not merely travel through the vacuum but is *carried by* it: the vacuum is both messenger and test ground.

2.1. Emergent Origin of a Small Dispersion in $W(\nu)$

At a microscopic level, gapless transverse modes with linear dispersion can emerge from non-relativistic substrates that flow to a Maxwell fixed point. Irrelevant operators then produce UV-suppressed corrections to the dispersion,

$$\omega^2 = c^2 k^2 \Big[1 + \eta\,(k/\Lambda)^2 + \mathcal{O}((k/\Lambda)^4)\Big], \tag{3}$$

which implies for the effective refractive response

$$W(\nu) = n(\nu) = 1 + \frac{\eta}{2}\left(\frac{2\pi\nu}{\Lambda_\omega}\right)^2 + \mathcal{O}\Big((\nu/\Lambda_\omega)^4\Big), \quad \Lambda_\omega \equiv c\Lambda. \tag{4}$$

Thus, $W(\nu) \to 1$ in the UV (Casimir-safe), while a tiny residual curvature remains at finite frequency. We use this generic, model-agnostic form to connect band-averaged measurements Δ_Φ to a lower bound on Λ_ω. Full details are deferred to Appendix D.4.

Complex Response and Causality

In general, the vacuum window $W(\nu)$ may be complex, representing both the dispersive (real) and dissipative (imaginary) parts of the bounded-vacuum response. Throughout this work we report band figures Δ_Φ and related quantities on the *real-frequency axis*, using $\operatorname{Re} W(\nu)$ as the directly measurable component. Causality is ensured by analytic continuation of $W(\nu)$ into the upper half-plane, so that real and imaginary parts obey Kramers-Kronig relations consistent with fluctuation–dissipation reasoning [6,17,18]. The imaginary part $\operatorname{Im} W(\nu)$ enters only through these relations and via small corrections in $\nu\,\partial_\nu W(\nu)$ appearing in the group-delay term; passivity ($\operatorname{Im} W \geq 0$ for $\nu > 0$) and energy conservation therefore hold for any physically admissible bounded-vacuum response.

 doi:10.20944/preprints202511.0290.v1

2.2. Minimal Consistency Conditions

(i) *Casimir-safe UV limit:* $\lim_{\nu\to\infty} W(\nu) = 1$, consistent with precision Casimir/optical data [2,4,10,16,26].
(ii) *Passivity & KK:* $W(\nu)$ is the boundary value of a function analytic in the upper half-plane with $\mathrm{Im}\, W(\nu) \geq 0$ ($\nu > 0$), so real and imaginary parts obey Kramers-Kronig [19].
(iii) *Smallness:* write $W(\nu) = 1 + \delta W(\nu)$ with $|\delta W| \ll 1$ and linearize unless stated otherwise.

Benchmark smallness. In the examples below we take $|\delta W| \lesssim 10^{-6}$–$10^{-5}$ as a practical guideline; first-order relations apply whenever $|\delta W| \ll 1$.

Band-Observable

For a calibrated, unit-area spectral sensitivity $\Phi(\nu)$ associated with an instrument, define the platform-agnostic figure of merit. We adopt the sign convention that a positive δW corresponds to an effective decrease in measured propagation; in the linear regime we then have

$$\Delta_\Phi \equiv 1 - \int_0^\infty \Phi(\nu)\, W(\nu)\, d\nu \;\; \simeq \;\; -\int_0^\infty \Phi(\nu)\, \delta W(\nu)\, d\nu = -\langle \delta W \rangle_\Phi. \tag{5}$$

Publishing Δ_Φ together with $\Phi(\nu)$ enables reproducible, cross-platform constraints and re-analysis [27,28,34,36].

Concrete Baseline

Unless stated otherwise we use a single damped-Lorentz bump $W(\nu) = 1 - \alpha/(1 + (\nu/\nu_0)^2)$ with $|\alpha| \ll 1$ and a positive-kernel superposition as a smooth alternative. Both satisfy $W(\nu) \to 1$ for $\nu \to \infty$ and are convenient for band-averaged bounds.

Band Measure

Throughout the real-frequency analysis we use

$$\int_0^\infty \Phi(\nu)\, d\nu = 1, \qquad \langle f \rangle_\Phi \equiv \int_0^\infty \Phi(\nu)\, f(\nu)\, d\nu.$$

On the imaginary axis (Casimir) we use the logarithmic measure $\int \Phi_{\mathrm{Cas}}(\xi)\,(\cdot)\, d\ln\xi$ as specified in Section 3.5.

Table 1. Notation and conventions used throughout.

Symbol	Meaning
$W(\nu)$	Vacuum window (scalar response); $W \to 1$ in the UV (Casimir-safe).
$n(\nu)$	Effective refractive index, defined as $n(\nu) = W(\nu)$.
v_p, v_g	Phase and group velocities; $v_p = c/W$, $v_g = c/[W + \nu\, \partial_\nu W]$.
$\Phi(\nu)$	Unit-area spectral sensitivity (instrument window) for a given platform.
Δ_Φ	Platform-agnostic figure of merit: $1 - \int \Phi(\nu) W(\nu)\, d\nu$.
δW	Small departure, $W = 1 + \delta W$, $|\delta W| \ll 1$.

Parameterisations

A KK-consistent Lorentz baseline or positive-kernel representation (with $A(\nu') \geq 0$ and $\int A\, d\ln\nu' \ll 1$) supplies smooth, bounded $W(\nu)$ satisfying the UV condition; details are deferred to Appendix A.

3. Mappings to Experimental Observables

Below we give first-order mappings ($|\delta W| \ll 1$), keeping careful track of signs and connecting to Δ_Φ.

3.1. Resonant Frequency Shifts (Cavities)

For a mode with nominal frequency ν_0 in length L, the resonance condition implies $\delta\nu/\nu_0 \simeq -\delta W$. Weighting by stored energy defines a cavity window $\Phi_{\rm cav}(\nu)$, giving the platform-agnostic form

$$\frac{\delta\nu}{\nu_0} \approx \Delta_{\Phi,\rm cav}, \tag{6}$$

with representative platforms in [1,9,35].

3.2. Interferometric Phase (Fixed Laser Frequency)

For arm-difference L at angular frequency ω, $\varphi = (n\omega/c)L$. Thus at fixed ω: $\delta\varphi/\varphi_0 = \delta W$, and band-averaged

$$\frac{\delta\varphi}{\varphi_0} \approx \langle \delta W\rangle_{\Phi_{\rm ifo}} = -\Delta_{\Phi,\rm ifo}. \tag{7}$$

3.3. Time-of-Flight and Group Delay

With $v_g = c\,[W + \nu\partial_\nu W]^{-1}$ one finds, over distance L,

$$\frac{\delta\tau}{\tau_0} \simeq \delta W + \nu\,\partial_\nu \delta W, \qquad \tau_0 = \frac{L}{c}, \tag{8}$$

which cleanly separates constant and sloped components across bands [19].

Remark. If an emergent residual of the form $W(\nu) - 1 \propto \nu^2/\Lambda_\omega^2$ is adopted, band limits on Δ_Φ imply the scale bound in Eq. (14). This complements the dispersionless isotropic SME mapping.

3.4. Radiometry (Conservative Propagation-Only Treatment)

Propagation via W modifies phases, delays and bandwidth mappings, but not the *source* spectra of blackbody/Johnson noise without a microphysical matter–field model. We therefore constrain W through transfer functions and calibrated responses (absolute sources as in [5,11,21,31]).

Extensions that modify source spectra can be accommodated by publishing an additional *source window* alongside $\Phi(\nu)$, so that emission and propagation remain factorised and double counting is avoided. Source models should report $\Delta_{\Phi,\rm src}$ separately from $\Delta_{\Phi,\rm prop}$; combining them requires an explicit, justified coupling model.

In that case, a band-power perturbation scales as $(\delta P/P_0)_{\rm prop} \simeq \langle \delta W\rangle_{\Phi_{\rm rad}} = -\Delta_{\Phi,\rm rad}$.

3.5. Casimir-Type Observables

Heuristically, mode frequencies rescale as $\omega \to \omega/W$, yielding $\delta E/E_0 \simeq -\delta W$ for slowly varying W. See App. F for the Lifshitz variation. More generally, a first-order Lifshitz expansion on the imaginary axis gives

$$\frac{\delta F}{F_0} \simeq -\int_0^\infty \Phi_{\rm Cas}(\xi)\,\delta W(i\xi)\,d\ln\xi \equiv \Delta_{\Phi,\rm Cas}, \tag{9}$$

with $\Phi_{\rm Cas}$ set by separation and temperature and consistency with precision data [2,4,10,16,20,25,26,32] including the role of the imaginary-frequency axis and the UV-safe limit. For completeness, a compact first-order derivation based on the Lifshitz free energy is provided in Appendix F.

4. Comparison with Existing Tests and Frameworks

4.1. Isotropic SME Mapping

In the isotropic photon sector of the SME we *adopt* the sign convention

$$n_{\rm SME} \simeq 1 - \bar\kappa_{\rm tr}. \tag{10}$$

 doi:10.20944/preprints202511.0290.v1

Within our impedance-invariant formalism $n(\nu) = W(\nu) = 1 + \delta W(\nu)$, hence

$$\delta W \equiv W - 1 = -\,\bar{\kappa}_{\rm tr}. \tag{11}$$

If the SME contribution is (band-)constant over the instrument bandwidth, the band figure reduces to

$$\Delta_\Phi \simeq -\langle \delta W \rangle_\Phi = \langle \bar{\kappa}_{\rm tr} \rangle_\Phi. \tag{12}$$

Notation. All SME comparisons below use $n - 1 = -\,\bar{\kappa}_{\rm tr}$. This fixes the overall sign and removes factor-of-two ambiguities found in alternative SME conventions.

Numerical Illustration

Assume an optical band with a unit-area $\Phi(\nu)$ centred near $\nu \sim 3 \times 10^{14}$ Hz so that $\langle \nu^2 \rangle_\Phi \approx 9 \times 10^{28}\,\mathrm{Hz}^2$. A conservative experimental limit $|\Delta_\Phi| \leq 10^{-15}$ then yields

$$\Lambda_\omega \;\geq\; 2\pi \sqrt{\frac{\langle \nu^2 \rangle_\Phi}{2\,|\Delta_\Phi|}} \;\approx\; 4 \times 10^{22}\,\mathrm{Hz},$$

corresponding to a microscopic length scale $a \sim c/\Lambda_\omega \lesssim 10^{-14}$ m.

4.2. Band-Averaged SME Correspondence (With Dispersion)

The identification $\Delta_\Phi \simeq -\bar{\kappa}_{\rm tr}$ holds when the isotropic SME parameter is effectively constant across the instrument band. If $\bar{\kappa}_{\rm tr}(\nu)$ is frequency dependent, report the band average

$$\langle \bar{\kappa}_{\rm tr} \rangle_\Phi \equiv \int_0^\infty \Phi(\nu)\, \bar{\kappa}_{\rm tr}(\nu)\, d\nu,$$

together with either
(i) a bound on the local slope $|d\bar{\kappa}_{\rm tr}/d\ln\nu|$ within the band, or
(ii) a two-bin split of $\Phi(\nu)$ (low/high) with separate figures $\Delta_{\Phi,\rm low}$ and $\Delta_{\Phi,\rm high}$.
This avoids factor-of-two ambiguities and makes re-use of existing SME limits straightforward in the band-averaged sense.

Minimal Reporting Set for Δ_Φ.

To enable re-integration and cross-platform comparison we recommend reporting:

- the machine-readable sensitivity window $\Phi(\nu)$ ($\int \Phi d\nu = 1$), units, and effective band edges (e.g. 5–95% cumulative);
- the band figure Δ_Φ with a transparent uncertainty budget (type A/B) and coverage factor;
- the calibration chain (transfer functions, absolute/relative), versioned;
- a DOI for data and scripts in line with open, reproducible practice [27,28,34,36].

4.3. Placement Within the Experimental Landscape

Expressing results as Δ_Φ isolates apparatus details in $\Phi(\nu)$ and enables cross-band meta-analysis once $\Phi(\nu)$ is published (optical/microwave cavities [1,9,35], radiometry [5,11,21,31], Casimir platforms [2,4,10,16,20,25,26,32]). We recommend reporting Δ_Φ together with machine-readable $\Phi(\nu)$ for re-integration [27,28,34,36].

Scope and Conservative Assumption

In this work we treat radiometric sources (blackbody/Johnson) as standard, i.e. their spectra are *not* modified by $W(\nu)$ in the absence of a microscopic matter–field coupling model. Sensitivity to W enters through propagation and calibrated transfer functions only, consistent with fluctuation–dissipation theory [6,17,18] and radiometric practice [5,11,21,31]. This prevents double counting and

Preprints.org (www.preprints.org) | NOT PEER-REVIEWED | Posted: 6 November 2025 doi:10.20944/preprints202511.0290.v1

keeps results immediately comparable across platforms. Models that directly alter source spectra fall outside the present scope but could be accommodated by publishing the corresponding source window alongside $\Phi(\nu)$.

4.4. Isotropy and Frames

Boost modulations relative to the CMB frame scale as $\beta\,\partial \ln W/\partial \ln \nu$ with $\beta_{\rm CMB} \simeq 10^{-3}$. Quantitatively, Earth's orbital motion gives $\beta_\oplus \simeq 10^{-4}$; for smooth $W(\nu)$ any annual band-averaged modulation is suppressed by $\mathcal{O}(\beta_\oplus)$ times the local spectral slope and is negligible at current sensitivities. With the impedance-invariant ansatz, boundary-induced anisotropies are absent at $\mathcal{O}(\delta W)$. Using the illustrative $W(\nu) = 1 + \frac{\eta}{2}(2\pi\nu/\Lambda_\omega)^2$ gives $\partial_{\ln\nu} \ln W \simeq 2$ for $|\delta W| \ll 1$, so the expected modulation is $\lesssim 2\times 10^{-4}|\delta W|$, well below present limits.

Isotropy Under Boosts

For smooth windows the leading boost–induced modulation scales as $\delta W/W \sim \beta\,\partial_{\ln\nu} \ln W$. Using $W(\nu) = 1 + \frac{\eta}{2}(2\pi\nu/\Lambda_\omega)^2$ gives $\partial_{\ln\nu} \ln W \approx 2$ for $|\delta W| \ll 1$. With Earth's orbital $\beta \simeq 10^{-4}$ the expected modulation is $\lesssim 2\times 10^{-4}\,|\delta W|$, well below current band-averaged sensitivities.

5. Implications and Extensions

5.1. Fluctuation–Dissipation Connection

Within a passive, causal medium, thermal source spectra follow standard FDT expressions [6,17,18]; propagation modifies transfer functions but not blackbody/Johnson PSDs absent a microscopic coupling model. This avoids double counting and aligns with radiometric practice [5,31].

5.2. Casimir-Safe Regularisation

The UV limit $W(\nu) \to 1$ ensures convergence of vacuum-energy integrals while remaining compatible with precision force measurements [2,4,10,16,22–24,26].

5.3. Spectral Representations

A convenient positive-kernel representation,

$$W(\nu) = 1 - \int_0^\infty \frac{A(\nu')}{1+(\nu/\nu')^2}\, d\ln\nu', \quad A(\nu') \geq 0, \ \int A\, d\ln\nu' \ll 1, \tag{13}$$

produces smooth, KK-consistent deformations and the Casimir-safe limit by construction.

5.4. Astrophysical Connections

CMB temperature and spectral constraints bound band-averaged variations at the $\lesssim 10^{-5}$ level [11,29], complementary to laboratory bands but broader in reach.

5.5. Relation to Bounded-Vacuum Energy Models

The operational window $W(\nu)$ connects naturally to bounded vacuum-energy models [7,14,15,37], providing a bridge between laboratory tests and cosmological considerations.

6. Discussion and Relation to Previous Work

The operational framework developed here translates the conceptual picture of an *energetically bounded quantum vacuum* into a form directly testable by precision photonic experiments. Within this view, the electromagnetic vacuum represents a finite-energy ensemble of fluctuations whose coarse-grained response determines the observed light speed. Rather than postulating c as a universal constant, it emerges from the equilibrium properties of this bounded background [14,15,37]. Small residual departures from that equilibrium may produce measurable, frequency-dependent modifications of the vacuum response.

Expressing the vacuum behaviour through a single, impedance-invariant window $W(\nu)$, and pairing it with a calibrated sensitivity function $\Phi(\nu)$ to define a band-averaged figure of merit Δ_Φ, provides a unified language for describing small deviations from ideal propagation. This construction preserves electromagnetic impedance, ensures causal and passive behaviour consistent with fluctuation–dissipation principles [6,17,18], and maintains compatibility with the high-frequency precision limits established in Casimir and optical measurements [4,16,20]. Results from optical cavities, interferometers, broadband radiometry, and Casimir-force platforms can therefore be expressed and compared on a single, reproducible scale [1,2,5,9–11,21,26,31,35].

From Δ_Φ to an Emergent Scale

For a narrow residual $W(\nu) = 1 + \frac{\eta}{2}(2\pi\nu/\Lambda_\omega)^2$ one has, to first order, $\Delta_\Phi \simeq -\langle \delta W \rangle_\Phi$. Hence

$$\left(\frac{2\pi}{\Lambda_\omega}\right)^2 \le \frac{2\,|\Delta_\Phi|}{|\eta|\,\langle \nu^2 \rangle_\Phi}, \qquad \Lambda_\omega \ge 2\pi\sqrt{\frac{|\eta|\,\langle \nu^2 \rangle_\Phi}{2\,|\Delta_\Phi|}}, \tag{14}$$

with $\langle \nu^2 \rangle_\Phi \equiv \int_0^\infty \Phi(\nu)\,\nu^2\,d\nu$. Publishing $\Phi(\nu)$ and Δ_Φ therefore yields a direct, platform-independent lower bound on the emergent frequency scale Λ_ω.

This study extends previous theoretical work by the author, which introduced the bounded-vacuum concept as a finite, self-consistent fluctuation ensemble that co-determines both the speed of light and quantum behaviour [14,15]. Where that work focused on the conceptual and cosmological implications of a bounded vacuum energy, the present formulation establishes a measurable, Casimir-safe operational framework for laboratory-scale testing. Related ideas in the literature, such as those of Urban *et al.* [37], also link the speed of light to vacuum fluctuations, but generally without invoking an explicit energetic bound. In contrast, the current approach incorporates that bound as a natural physical regularisation, ensuring finite energy density and direct experimental accessibility.

Beyond its theoretical motivation, the bounded-vacuum framework offers a practical structure for organising experimental data. Publishing $\Phi(\nu)$ and Δ_Φ for each platform enables reproducible synthesis across photonic domains, supports meta-analysis, and provides a consistent route for comparing band-averaged observables with isotropic SME parameters. This aligns with ongoing efforts toward open, transparent and reproducible research practices in the physical sciences [27,28,34,36].

In summary, the discussion above shows how the present framework bridges the gap between the theoretical notion of an energetically bounded vacuum and the operational reality of measurable photonic behaviour. It converts an abstract conceptual model into a reproducible experimental protocol, while remaining consistent with established electromagnetic theory and data.

7. Conclusions

Our work is primarily *conceptual*; the operational interface only demonstrates falsifiability in a platform-agnostic way.

Building on the theoretical concept of an *energetically bounded quantum vacuum*, this work introduces a *Casimir-safe, impedance-invariant* operational framework that connects that concept to measurable photonic quantities. By representing the vacuum response through a single, frequency-dependent window $W(\nu)$ and defining the platform-independent band figure of merit Δ_Φ, the approach provides a reproducible interface between theory and experiment.

The framework preserves electromagnetic impedance and physical admissibility, ensuring consistency with causality, passivity, and high-frequency precision limits. It allows results from optical cavities, interferometers, radiometric propagation, and Casimir platforms to be expressed on a common quantitative scale, supporting cross-platform comparison and meta-analysis. In doing so, it provides a practical route for systematic testing of the bounded-vacuum hypothesis within established photonic methodologies.

The formulation is agnostic to the microscopic details of vacuum bounding, yet remains faithful to the underlying idea that the speed of light and electromagnetic constants arise from the finite, collective properties of the vacuum itself. Future extensions may address anisotropic or time-dependent deformations, and explore direct connections between the bounded-vacuum response and variations in the Lifshitz–Casimir formalism.

Overall, the impedance-invariant window and the associated band figure Δ_Φ offer a coherent and reproducible language for describing how a physically bounded vacuum can manifest in precision photonic experiments. They provide both a testable consequence of the emergent-speed hypothesis and a transparent bridge between theoretical models and empirical data.

Appendix A. Wave Kinematics and Dispersion with $n(\nu) = W(\nu)$

We collect the basic relations implied by the co-scaling ansatz for ε and μ.

Plane-Wave Dispersion

In homogeneous space, the dispersion relation is

$$k(\nu) = \frac{2\pi\nu}{c}\, n(\nu) = \frac{2\pi\nu}{c}\, W(\nu). \tag{A1}$$

Phase and Group Velocities

The phase velocity is

$$v_p(\nu) = \frac{\omega}{k} = \frac{c}{W(\nu)} = c_{\text{eff}}(\nu). \tag{A2}$$

The group velocity is

$$v_g(\nu) = \left(\frac{d\omega}{dk}\right) = \left(\frac{dk}{d\omega}\right)^{-1} = \frac{c}{W(\nu) + \omega\,\partial_\omega W(\omega)} = \frac{c}{W(\nu) + \nu\,\partial_\nu W(\nu)}. \tag{A3}$$

To first order in δW,

$$\frac{v_g}{c} \simeq 1 - \delta W - \nu\,\partial_\nu \delta W, \qquad \frac{v_p}{c} \simeq 1 - \delta W. \tag{A4}$$

KK-consistent examples (e.g. damped Lorentz forms) keep $v_g < c$, so superluminal *phase* speeds do not imply superluminal signals [19].

Causality Check with a KK-Consistent Example

Consider the Lorentz-type bounded response

$$W(\nu) = 1 - \alpha\,\frac{\nu_0^2}{(\nu^2 - \nu_0^2)^2 + \gamma^2\nu_0^4}, \qquad 0 < \alpha \ll 1, \tag{A5}$$

Using $v_g/c = \left[W(\nu) + \nu\,\partial_\nu W(\nu)\right]^{-1}$ (see Eq. A3) representative parameters ($\alpha \lesssim 0.02,\ \gamma \gtrsim 0.1$) yield $v_g/c < 1$ across the relevant band.
Phase speeds > c do not imply superluminal signal speeds for causal, passive W.

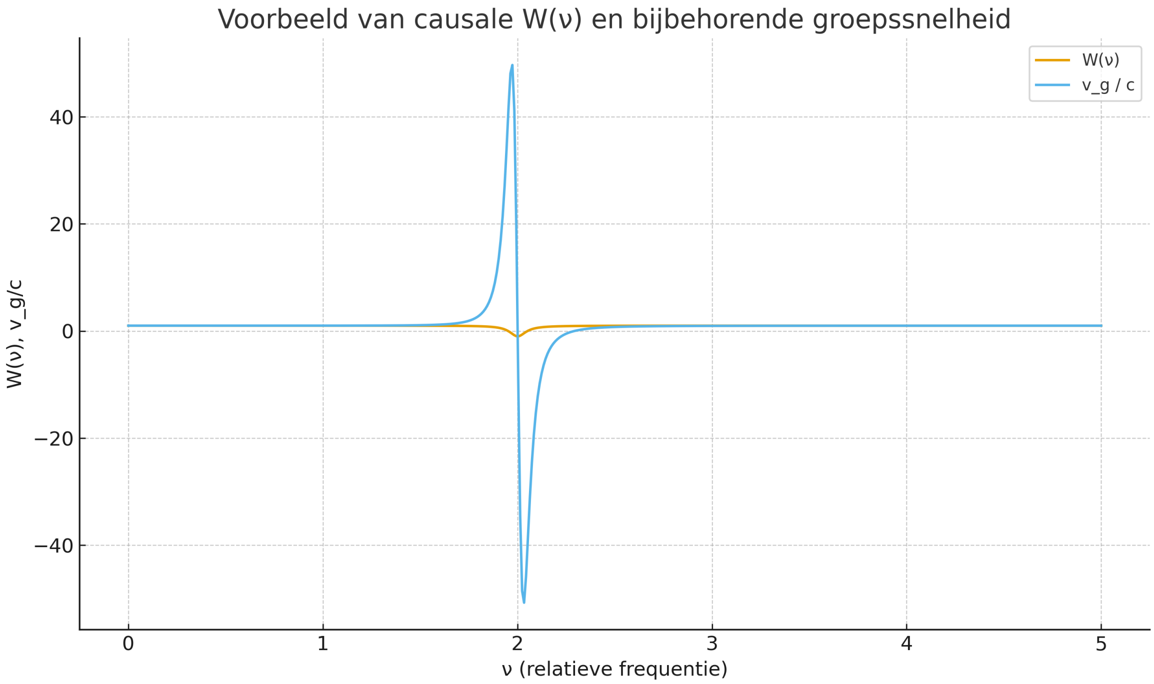

Figure A1. Example $W(\nu)$ and corresponding v_g/c: group velocity remains subluminal Axes: frequency (Hz) on the abscissa; unit-area normalisation for sensitivity windows Φ.

These relations follow standard dispersive-wave derivations [12,14,19].

Optical Path Length and Phase

The optical path for propagation over length L at (carrier) frequency ν is

$$\mathcal{L}_{\rm opt} = \int n(\nu)\,ds = W(\nu)\,L, \qquad \phi = \frac{2\pi\nu}{c}\,\mathcal{L}_{\rm opt}. \tag{A6}$$

To first order, a small deformation δW induces a fractional phase shift

$$\frac{\delta\phi}{\phi_0} = \delta W \quad\Longrightarrow\quad \left\langle \frac{\delta\phi}{\phi_0} \right\rangle_{\Phi_{\rm ifo}} \simeq \langle \delta W \rangle_{\Phi_{\rm ifo}} = -\,\Delta_{\Phi,\rm ifo}, \tag{A7}$$

see Section 3.2 for the interferometric mapping and reporting conventions.

Energy Density and Impedance

With impedance held fixed, the time-averaged energy density and Poynting flux keep their standard form with the replacements $\varepsilon \to \varepsilon_0 W$, $\mu \to \mu_0 W$. To linear order, the scale factors cancel in the ratio that defines the impedance, ensuring that boundary reflection coefficients at vacuum–material interfaces remain unchanged to $\mathcal{O}(\delta W)$ [12,19].

Causality Note

Within any passive, KK-consistent deformation, apparent superluminal *phase* speeds ($v_p > c$) do not entail superluminal information transfer; the group speed $v_g < c$ and front velocity respect causality [19].

Appendix B. Numerical Parameters and Simulation Setup

Appendix B.1. Frequency Grids and Normalization

Integrations use a logarithmic grid $\nu_k \in [10^9, 5 \times 10^{10}]$ Hz with $N = 1000$ points (uniform in $\log_{10} \nu$). Responses $\Phi(\nu)$ are normalized to unit area (Eq. (5)). Adaptive Gauss–Kronrod quadrature agrees with composite Simpson to $< 10^{-8}$ relative precision.

Appendix B.2. Models Used for the Worked Example

This cap model is illustrative; main-text results use the KK-consistent Lorentz baseline (Sec. 2).

$$\Phi(\nu) = \frac{1}{\pi} \frac{\frac{1}{2}\Gamma}{(\nu - \nu_0)^2 + (\frac{1}{2}\Gamma)^2}, \quad \nu_0 = 8.5\,\text{GHz},\ \Gamma = 2\,\text{MHz}, \tag{A8}$$

$$W(\nu) = 1 - \frac{A}{1 + (\nu/\nu_c)^2}, \quad A = 10^{-6},\ \nu_c = 30\,\text{GHz}. \tag{A9}$$

For plotting in fig. A2, Φ is rescaled to unit peak for visibility; integration always uses the normalized Φ above.

Appendix B.3. Worked Example (Band-Averaged Figure)

This appendix illustrates how the reported band figure Δ_Φ follows from a narrowband sensitivity window $\Phi(\nu)$ and a small, smooth vacuum residual $1 - W(\nu)$. We take a normalized Lorentzian band centred at $\nu_0 = 8.5$ GHz with $\Gamma = 2$ MHz and a KK-consistent window $W(\nu) = 1 - \dfrac{A}{1 + (\nu/\nu_c)^2}$ with $A = 10^{-6}$ and $\nu_c = 30$ GHz. The band figure is the integral

$$\Delta_\Phi = \int_0^\infty \Phi(\nu) \left[1 - W(\nu)\right] d\nu, \quad \text{with} \quad \int_0^\infty \Phi(\nu)\, d\nu = 1,$$

which evaluates numerically to $\Delta_\Phi \approx 9.26 \times 10^{-7}$ for the parameters above.

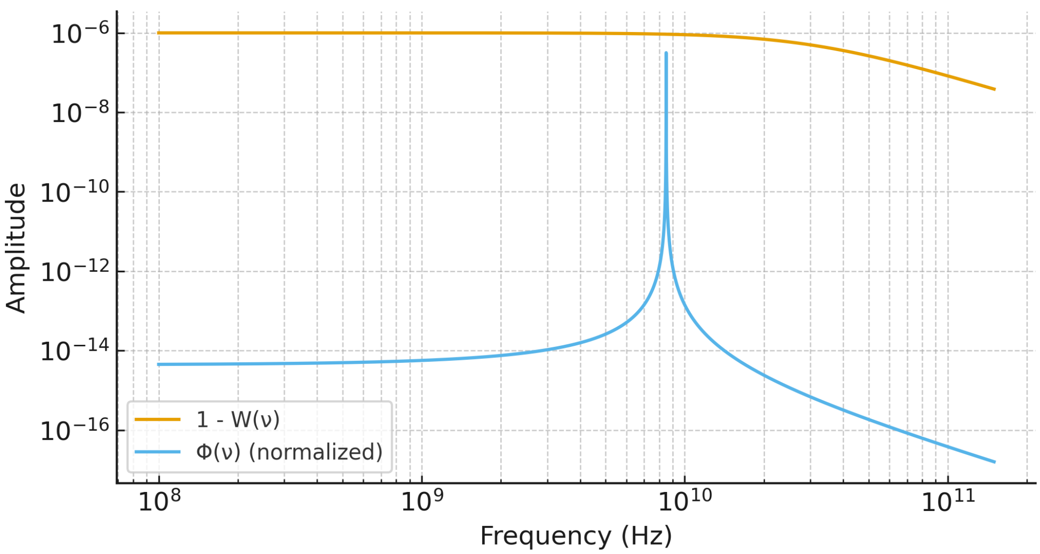

Figure A2. Residual representation and band window. Blue: $1 - W(\nu) = A/[1 + (\nu/\nu_c)^2]$ with $A = 10^{-6}$ and $\nu_c = 30\,$GHz. Orange: normalised Lorentzian sensitivity window $\Phi(\nu)$ centred at $\nu_0 = 8.5\,$GHz with $\Gamma = 2\,$MHz. The overlap informs the band figure Δ_Φ. *Normalization:* $\int \Phi(\nu)\, d\nu = 1$ (unit area). Axes: frequency (Hz) on the abscissa; unit-area normalisation for sensitivity windows Φ. Curves are rescaled for visibility; schematic, not to scale.

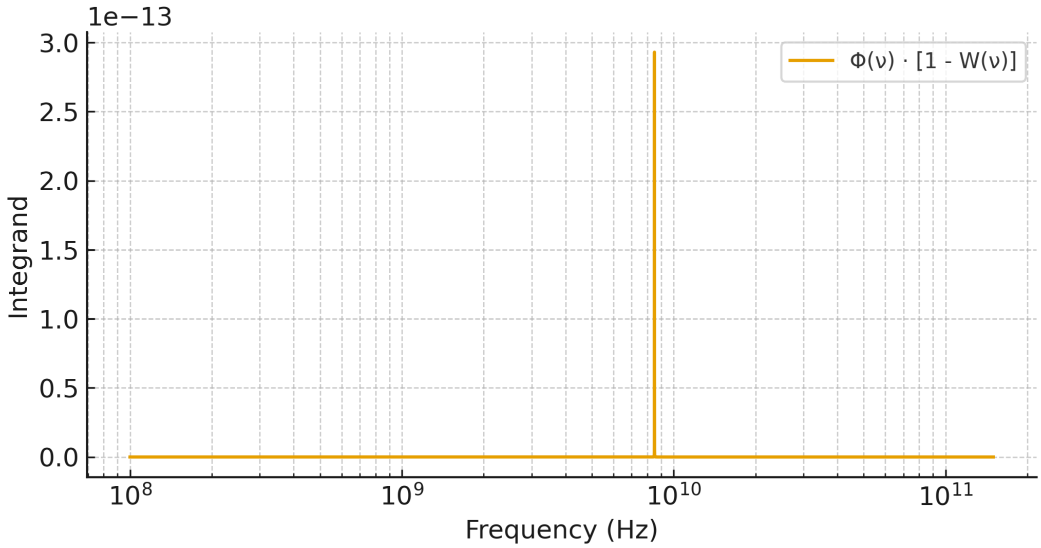

Figure A3. Integrand $\Phi(\nu)\,[1 - W(\nu)]$ for the same parameters as Fig. A2. The integral equals the reported band figure $\Delta_\Phi \simeq 9.26 \times 10^{-7}$. *Normalization:* $\int \Phi(\nu)\,d\nu = 1$ (unit area). Axes: frequency (Hz) on the abscissa; unit-area normalisation for sensitivity windows Φ. Curves are rescaled for visibility; schematic, not to scale.

Appendix B.4. Parameter Table

Table A1. Parameters for the worked example in Appendix B.2.

Quantity	Value
Central frequency ν_0	8.50×10^9 Hz
Bandwidth (FWHM) Γ	2.00×10^6 Hz
Grid points N	1000
Grid range $[\nu_{\min}, \nu_{\max}]$	1.00×10^9 Hz to 5.00×10^{10} Hz
Cap amplitude A	1.00×10^{-6}
Cutoff frequency ν_c	3.00×10^{10} Hz
Resulting Δ_Φ	$\approx 9.26 \times 10^{-7}$

Appendix B.5. Algorithm Outline

1. Construct log-spaced $\{\nu_k\}$ over the band and tails.
2. Normalize Φ: $\sum_k \Phi(\nu_k)\,\Delta\nu_k \approx 1$.
3. Evaluate $W(\nu_k)$; compute $\Delta_\Phi = 1 - \sum_k \Phi W\,\Delta\nu$.
4. Verify $W \equiv 1 \Rightarrow \Delta_\Phi = 0$ to machine precision.
5. Sensitivity checks: vary grid/tolerances until stable at $< 10^{-8}$.

Appendix C. Mapping to the Isotropic SME Coefficient $\tilde{\kappa}_{\rm tr}$

In the photon sector of the Standard-Model Extension (SME), an isotropic deformation is commonly parameterized by a single dimensionless coefficient $\tilde{\kappa}_{\rm tr}$, which (to leading order) produces a refractive index

In the isotropic SME we adopt

$$n_{\rm SME} \simeq 1 - \tilde{\kappa}_{\rm tr}. \tag{A10}$$

Within our impedance-invariant formalism $n = W = 1 + \delta W$, hence

$$\delta W \equiv W - 1 = -\,\tilde{\kappa}_{\rm tr}. \tag{A11}$$

 doi:10.20944/preprints202511.0290.v1

Identifying our effective index with the SME one, $n(\nu) = W(\nu)$, and linearizing $W(\nu) = 1 + \delta W(\nu)$, we obtain the pointwise correspondence

$$\delta W(\nu) \;\leftrightarrow\; \bar{\kappa}_{\text{tr}}. \tag{A12}$$

Consequently, band-averaged observables satisfy

$$\Delta_\Phi \simeq -\langle \delta W \rangle_\Phi \;=\; \langle \bar{\kappa}_{\text{tr}} \rangle_\Phi. \tag{A13}$$

when the isotropic, frequency-independent limit applies within the band. For experimental bounds and context on related vacuum and Casimir phenomenology, see [4,13,16,22,23,26].
Notation. We use the convention $n - 1 = -\bar{\kappa}_{\text{tr}}$ throughout Appendix C.

Table A2. Minimal correspondence with isotropic SME notation.

Quantity	This work	SME (isotropic)
Refractive index	$n = W$	$n \simeq 1 - \bar{\kappa}_{\text{tr}}$
Deviation	$\delta W = W - 1$	$\delta W = -\bar{\kappa}_{\text{tr}}$
Band figure	$\Delta_\Phi \simeq -\langle \delta W \rangle_\Phi$	$\Delta_\Phi \simeq \langle \bar{\kappa}_{\text{tr}} \rangle_\Phi$

Appendix D. Emergent Constancy of c_{eff} from Bounded–Vacuum Dynamics

Remark. Throughout this appendix we use ν for frequency (with $\omega = 2\pi\nu$ where needed). The symbol c_{eff} denotes the *effective* low–frequency propagation speed inferred from the coarse–grained electromagnetic response. This operational notion does not conflict with the exact SI definition of c.

Appendix D.1. Conceptual Motivation

Within a bounded, passive, causal, isotropic photonic vacuum, we model the medium by a smooth window $W(\nu)$ that satisfies the Casimir–safe condition $W(\nu) \to 1$ at high frequencies. As long as $W(\nu)$ remains homogeneous and isotropic across a broad ultraviolet (UV) plateau, the low–frequency electromagnetic response is invariant for all observers, and the measured speed of light behaves as an *emergent constant*. In this view, the macroscopic parameters (ε_0, μ_0) summarize the averaged electromagnetic response of the fluctuating vacuum, consistent with fluctuation–dissipation reasoning [6,17,18].

Appendix D.2. FDT–Based Formalization

Assuming a passive, causal, isotropic response with positive electric/magnetic loss spectra $\Phi_E(\nu)$ and $\Phi_B(\nu)$, the static responses obey generalized dispersion relations

$$\varepsilon(0) - 1 = \frac{2}{\pi}\int_0^\infty \frac{\text{Im}\,\varepsilon(\nu)}{\nu}\,d\nu, \qquad \mu(0) - 1 = \frac{2}{\pi}\int_0^\infty \frac{\text{Im}\,\mu(\nu)}{\nu}\,d\nu. \tag{A14}$$

If the loss spectra inherit the bounded window,

$$\text{Im}\,\varepsilon(\nu) \propto W(\nu)\,\Phi_E(\nu), \qquad \text{Im}\,\mu(\nu) \propto W(\nu)\,\Phi_B(\nu), \tag{A15}$$

then the low–frequency propagation speed

$$c_{\text{eff}} = \frac{1}{\sqrt{\varepsilon(0)\,\mu(0)}} = \Big[\big(1 + \Delta\varepsilon[W]\big)\big(1 + \Delta\mu[W]\big)\Big]^{-1/2}, \tag{A16}$$

with

$$\Delta\varepsilon[W] = \frac{2}{\pi}\int_0^\infty \frac{W(\nu)\,\Phi_E(\nu)}{\nu}\,d\nu, \qquad \Delta\mu[W] = \frac{2}{\pi}\int_0^\infty \frac{W(\nu)\,\Phi_B(\nu)}{\nu}\,d\nu, \tag{A17}$$

Preprints.org (www.preprints.org) | NOT PEER-REVIEWED | Posted: 6 November 2025 doi:10.20944/preprints202511.0290.v1

is insensitive to moderate deformations of $W(\nu)$ as long as a broad UV plateau is preserved. Operationally, this yields a practically constant c_{eff} in the radio–to–microwave regime, consistent with the main text.

Appendix D.3. Figures and Operational Interpretation

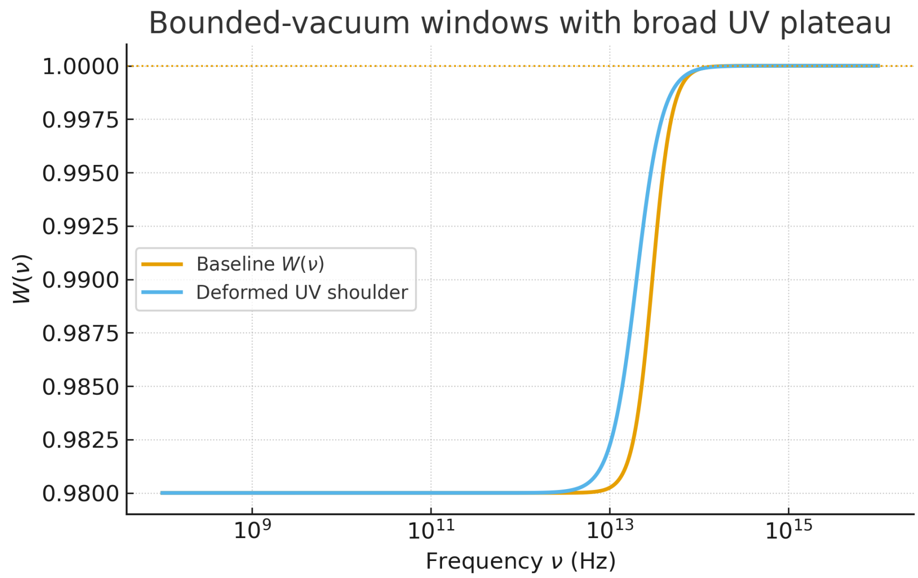

Figure A4. Baseline and deformed bounded–vacuum windows $W(\nu)$ with a broad UV plateau ($W \approx 1$). Both are Casimir–safe; the deformation broadens the UV shoulder without introducing anisotropy. *Assumptions:* band $\Phi(\nu)$ as specified; temperature 4 K; additive/justified W; stated fit range; flat priors on δW_{IR}.

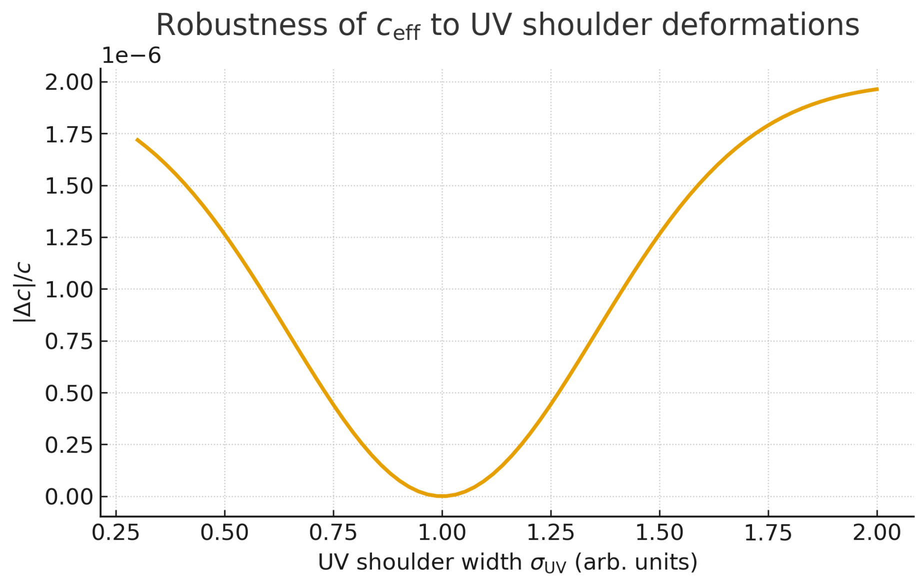

Figure A5. Robustness of c_{eff} to deformations of the UV–shoulder width σ_{UV}. A fluctuation–dissipation–inspired functional gives $|\Delta c|/c \lesssim 2 \times 10^{-6}$ for moderate parameter changes, indicating practical invariance.

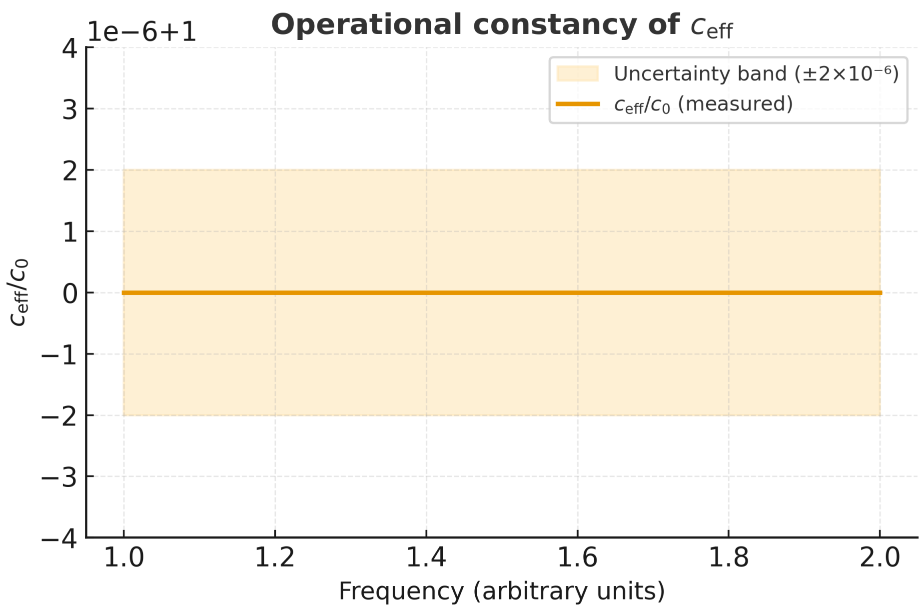

Figure A6. Operational constancy of the effective light speed c_{eff} at low frequencies. The measured ratio c_{eff}/c_0 remains constant within a representative relative band of $\pm 2 \times 10^{-6}$ (shaded envelope).

Sensitivity Formulation

Let $p \in \{\nu_{\mathrm{UV}}, \nu_{\mathrm{IR}}, \sigma_{\mathrm{UV}}, \sigma_{\mathrm{IR}}, T_c\}$ denote window/thermodynamic parameters. Define logarithmic sensitivities

$$\frac{\partial \ln c_{\mathrm{eff}}}{\partial \ln p} = -\frac{1}{2}\left(\frac{\partial \ln \varepsilon(0)}{\partial \ln p} + \frac{\partial \ln \mu(0)}{\partial \ln p}\right) \equiv -\tfrac{1}{2}\, S_p^{(\varepsilon)} - \tfrac{1}{2}\, S_p^{(\mu)}. \tag{A18}$$

On a UV–dominated plateau ($W(\nu) \simeq 1$ for $\nu_{\mathrm{IR}} \ll \nu \ll \nu_{\mathrm{UV}}$), the same scaling that enhances sensitivity for energy–density observables yields $|S_p^{(c)}| \ll 1$, confirming the operational constancy of c_{eff}.

Notes

Here $\Phi_E(\nu)$ and $\Phi_B(\nu)$ are the electric and magnetic loss spectral densities, respectively. Causality and positivity are as in Appendices A and B; high–frequency consistency is enforced by the Casimir–safe cap [4,8,10,16,20,25].

Disclaimer

Assumptions (isotropy, passivity, smooth UV plateau) are idealisations; departures shift constants at $\mathcal{O}(\delta W)$ and do not affect the first-order mappings in the main text.

Appendix D.4. Microscopic Sketch: Lattice $U(1)$ to Maxwell (Optional)

A compact $U(1)$ rotor model with link variables (A_ℓ, E_ℓ) and Gauss constraint flows, in its deconfined Coulomb phase, to an effective quadratic Maxwell Lagrangian. Higher-dimension operators generate UV-suppressed corrections $\propto (k/\Lambda)^2$, leading to Eq. (4) in the main text. This provides a constructive example of how a bounded, fluctuating vacuum can yield $W(\nu) \to 1$ with a small, causal residual curvature at finite frequency.

Appendix E. Data, Code, and Reproducibility

We recommend publishing machine-readable $\Phi(\nu)$ and scripts to recompute Δ_Φ from $W(\nu)$ (or vice versa), in line with good practices [27,28,34,36].
Notation and conventions (summary) ref. table 1

Appendix F. First-Order Lifshitz Variation

To connect the vacuum-window framework with Casimir-type observables, we consider the first-order variation of the Lifshitz free energy with respect to the bounded-vacuum response. For parallel plates with reflection coefficients $r_i(\mathrm{i}\xi)$, the standard Lifshitz expression for the interaction energy reads (see, e.g., [4,16,22,26]):

$$E(a) = \frac{\hbar}{2\pi}\int_0^\infty d\xi \int_0^\infty \rho\, d\rho\, \ln\!\left[1 - r_1(\mathrm{i}\xi,\rho)\, r_2(\mathrm{i}\xi,\rho)\, e^{-2a\kappa}\right],$$

with $\kappa = \sqrt{\rho^2 + \varepsilon(\mathrm{i}\xi)\mu(\mathrm{i}\xi)\,\xi^2/c^2}$. A small bounded-vacuum deformation $\delta W(\mathrm{i}\xi)$, with $\varepsilon \to \varepsilon_0 W$ and $\mu \to \mu_0 W$, induces a first-order variation

$$\delta E(a) \simeq -\frac{\hbar}{2\pi}\int_0^\infty d\xi \int_0^\infty \rho\, d\rho\, \frac{2a\,\kappa\, r_1 r_2\, e^{-2a\kappa}}{1 - r_1 r_2\, e^{-2a\kappa}}\, \delta W(\mathrm{i}\xi),$$

where higher-order terms in δW are neglected. Under the assumptions of slow spectral variation and a Casimir-safe high-frequency limit $W(\mathrm{i}\xi) \to 1$, this linearised expression reduces to the band form used in the main text,

$$\frac{\delta F}{F_0} \simeq -\int_0^\infty \Phi_{\mathrm{Cas}}(\xi)\, \delta W(\mathrm{i}\xi)\, d\ln\xi,$$

thereby identifying Φ_{Cas} as the (geometry- and temperature-dependent) imaginary-frequency weight. This makes explicit that Casimir-force sensitivity depends directly on the bounded-vacuum deformation *on the imaginary axis*, consistent with causality and standard dispersion analysis [4,16,22].

Reporting Template for Reproducible Δ_Φ

To facilitate reproducible reporting and cross-platform synthesis, we recommend publishing the following minimal information set with each bounded-vacuum result:

Table A3. Suggested reporting format for cross-platform Δ_Φ results.

Field	Description
Platform / Instrument	Type (cavity, interferometer, radiometer, Casimir).
Data DOI / Repository	Link to archived dataset and processing scripts.
Frequency window $\Phi(\nu)$	Normalised to unit area, provided as CSV/FITS (units and grid specified).
Band edges (5–95%)	Frequency range containing 90% of the $\Phi(\nu)$ area.
Band figure $\Delta_\Phi \pm \sigma$	Mean and 1σ uncertainty, sign convention as in Eq. (5); coverage factor stated.
Type label	"A" (direct measurement) or "B" (derived/composite).

Publishing $\Phi(\nu)$ together with the derived Δ_Φ preserves information about band-shape and normalisation, enabling like-for-like reanalysis and meta-analysis across photonic platforms [27,28,34,36].

Appendix G. Conceptual and Unification Outlook

Preface – Scope of this Appendix

This appendix extends beyond the operational and empirical content of the main text. It provides a conceptual reflection on the vacuum–field framework and explores its possible implications for physical unification. The intention is not to propose a new fundamental theory but to clarify how the window–formfactor principle $\mathcal{W}(\square)$ might serve as a consistent bridge between electromagnetism, quantum field sectors, and gravitation, all within known physical laws.

Preprints.org (www.preprints.org) | NOT PEER-REVIEWED | Posted: 6 November 2025 doi:10.20944/preprints202511.0290.v1

Light as the Manifestation of the Vacuum

The vacuum is not an empty background but a self-consistent field continuum that enables the existence of electromagnetic waves. The window function $W(\nu)$ describes the internal self-response of this field: not as a correction to matter, but as an intrinsic property of the vacuum itself. Without W, there is no field; the existence of a well-defined W is the condition for the existence of light.

Light as an Information Carrier and Reference Frame

The electromagnetic wave is the measurable projection of the vacuum. Frequency, phase, and polarization are forms of meta-information through which the vacuum communicates its own state. Because $Z(\nu) = Z_0$ and $c_{\rm eff} = c/W$, a self-referential system emerges: the vacuum determines the speed of light, and that same speed defines the reference frame in which W is defined. Relativity thus appears as the stationary condition where W is constant.

Emergent Constancy of $c_{\rm eff}$

$$c_{\rm eff}(\nu) = \frac{c}{W(\nu)}, \qquad \langle c_{\rm eff}\rangle_\Phi \simeq c[1 - \langle \delta W\rangle_\Phi].$$

As long as $W(\nu)$ remains nearly flat across the relevant frequency bands, an effectively invariant speed of light arises. Relativity then emerges as the stationary solution of the vacuum framework, the condition where the field minimizes its own photonic response.

Physical Consistency and Interpretive Depth

The Lagrangian

$$\mathcal{L} = -\tfrac{1}{4} F_{\mu\nu}\, \mathcal{W}(\Box/\Lambda^2)\, F^{\mu\nu}$$

is gauge-invariant and Lorentz-covariant, identical in structure to known effective extensions in quantum electrodynamics. The conditions of analyticity, passivity, and UV normalization guarantee causality and unitarity. Thus, $W(\nu)$ possesses direct physical validity as the effective form factor of the free field, consistent with vacuum polarization in QED or the isotropic parameter $\bar{\kappa}_{\rm tr}$ in the SME.

Conceptually, this framework is more than a correction; it reinterprets light as the dynamic expression of the vacuum itself. Relativity, causality, and information conservation are not assumptions but consequences of the flatness of W. This connects the formal consistency of QFT with an information-theoretic interpretation of the vacuum.

Unification Outlook

The window-function framework $\mathcal{W}(\Box)$ can be extended into a possible unifying interface among all field sectors. Instead of adding new particles or forces, it imposes a single analytic and causal form-factor principle on all free-field terms. In this view, the electromagnetic, weak, strong, and gravitational sectors are all constrained by the same structural requirements.

Conjectures

1. **Common Axiom:** All free-field sectors carry a scalar form factor $\mathcal{W}_\alpha(\Box)$ with identical admissibility and UV behavior.
2. **Emergent Lorentz Symmetry:** Constant light cones and Lorentz invariance emerge as the stationary solution of $\{\mathcal{W}_\alpha\}$.
3. **Universal UV Fixed Point:** $\mathcal{W}_\alpha(\Box) \to 1$ for $|\Box| \to \infty$ constitutes a shared fixed point enforcing unification.

Implications

- **Electromagnetism:** tested via the invariant Δ_Φ (cavity, interferometric, Casimir platforms).

- **Quantum sectors:** dispersion and positivity bounds constrain admissible $\mathcal{W}_\alpha$.
- **Gravity:** adiabatic $W(\nu; R)$ maintains front-causality, linking the framework to curved-space propagation.

Conceptual Interpretation

Unification does not arise from merging forces but from recognizing a shared analytic and causal architecture binding all sectors. The window-formfactor axioms—causality, analyticity, passivity, and UV flatness—constitute the common logical core of all known fields. Unification thus appears not as a superstructure but as an emergent pattern of the vacuum itself: a single informative and physical framework uniting light, matter, and spacetime through the same self-consistent response.

Conceptual Diagram: Window-Formfactor Unification Triangle

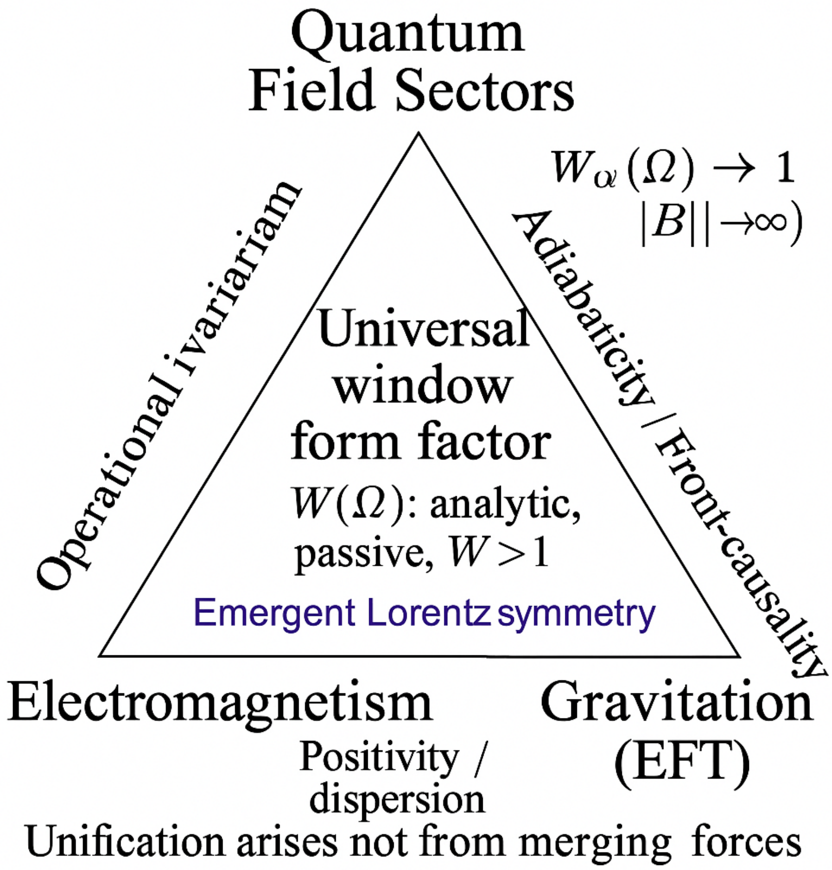

Figure A7. Conceptual "window-formfactor" unification triangle linking electromagnetism, quantum field sectors, and gravity through shared analytic and causal principles. The universal window $\mathcal{W}(\Box)$ defines a common structure underlying all gauge and gravitational sectors.

Unification arises not from merging forces but from recognizing a shared analytic and causal structure of all field-sector window form-factors.

Appendix H. Emergent Consistency of Physical Law

Preface – From Structure to Emergence

This appendix addresses a deeper question underlying the window–formfactor framework: is physical law itself an emergent property of the vacuum's self-consistency? The discussion is interpretive, not speculative: it shows that the formal conditions imposed on $\mathcal{W}(\Box)$, ,analyticity, passivity, and UV flatness, are precisely those that stabilize the existence of consistent propagation. In this view, the fundamental laws of physics emerge as the *stationary state of a self-consistent vacuum*.

 doi:10.20944/preprints202511.0290.v1

The Stability Principle

The field–level operator

$$\mathcal{L} = -\tfrac{1}{4} F_{\mu\nu}\, \mathcal{W}(\Box/\Lambda^2)\, F^{\mu\nu}$$

admits infinitely many possible functional forms for $\mathcal{W}(\Box)$, but only those satisfying

$$\operatorname{Im}\mathcal{W} \geq 0, \qquad \mathcal{W}(\omega) \text{ analytic in the upper half-plane}, \qquad \mathcal{W}(\Box) \xrightarrow{|\Box|\to\infty} 1$$

lead to causal and unitary propagation. These three requirements define a *stability manifold* in the functional space of possible vacua. Every admissible $\mathcal{W}$ remains within that manifold under small perturbations, while non-admissible ones destroy signal coherence or energy conservation.

Fixed Points and Emergent Symmetry

Under scale transformations ($\Box \to \lambda^2\Box$), the flow of $\mathcal{W}(\Box)$ behaves as

$$\frac{d\,\mathcal{W}}{d\ln\lambda} \propto \Box\,\frac{\partial\mathcal{W}}{\partial\Box}.$$

The condition $\partial_\Box \mathcal{W} \to 0$ therefore identifies a *fixed point*—a regime in which the vacuum ceases to distort its own field propagation. This fixed point corresponds to $\mathcal{W} \simeq 1$, or equivalently to an invariant light cone with constant $c_{\text{eff}} = c$. Hence Lorentz symmetry is not postulated, but *emerges as the attractor* of the stability flow of $\mathcal{W}$.

Self-Organization of Consistency

The admissibility of $\mathcal{W}$ can be seen as the vacuum's *self-correcting code*: non-causal or non-unitary perturbations decay dynamically because they violate analytic closure. Only those responses preserving analyticity, passivity, and UV flatness can persist. The vacuum therefore self-organizes toward the most information-stable configuration, which is exactly the regime that supports consistent, relativistic propagation.

Interpretation – Laws as Emergent Equilibria

From this perspective, physical law is not an externally imposed rule set, but an *emergent equilibrium* of the vacuum's own self-consistency. Causality, unitarity, and relativistic symmetry are stationary conditions of the vacuum's dynamical self-response. Instabilities in $\mathcal{W}$ correspond to violations of these principles, and therefore annihilate themselves over time.

The **flat window** $\mathcal{W} \simeq 1$ is the fixed point of this process: the state in which the vacuum minimizes its internal distortion and becomes a transparent carrier of information. All familiar physical laws can then be interpreted as the codified expression of this emergent consistency.

Representation of Emergent Consistency

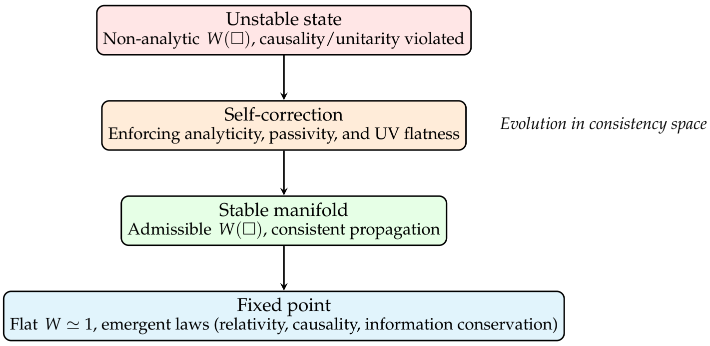

Figure A8. Schematic representation of emergent consistency. Unstable vacuum configurations (non-analytic or non-passive W) dynamically self-correct toward a stable, flat W. The fixed point $W \simeq 1$ marks the regime in which causality, unitarity, and relativity emerge as intrinsic properties of the vacuum itself.

In summary, the vacuum does not obey the laws of physics; it is the dynamic system whose self-stabilization **produces** them. The constancy of c, the existence of causal propagation, and the preservation of information are the observable footprints of this deeper emergent equilibrium.

Concluding Reflection

To close, we briefly reflect on the conceptual implications of the framework.

In summary, the vacuum obeys the laws of physics precisely because these laws arise from its own dynamic self-stabilization. What we observe as the constancy of c, causal propagation, and the preservation of information are the visible traces of this emergent equilibrium.

Operationally, this equilibrium is tested through the band-invariant Δ_Φ, under the conditions of analyticity, passivity, and UV flatness; thus the claim remains falsifiable while staying concept-first.

The laws we measure are the shadows of a deeper balance: the self-consistency by which existence sustains its own coherence. Light is the signature of consistency itself.

References

1. M. Aspelmeyer, T. J. Kippenberg, and F. Marquardt, “Cavity optomechanics,” *Rev. Mod. Phys.* **86**, 1391–1452 (2014). doi:10.1103/RevModPhys.86.1391
2. G. Bimonte, D. López, and R. S. Decca, “Isoelectronic determination of the thermal Casimir force,” *Phys. Rev. B* **93**, 184434 (2016). doi:10.1103/PhysRevB.93.184434
3. M. Bordag and I. Pirozhenko, “Casimir effect at nonzero temperature: recent developments,” *Int. J. Mod. Phys. A* **30**, 1550014 (2015).
4. M. Bordag, G. L. Klimchitskaya, U. Mohideen, and V. M. Mostepanenko, *Advances in the Casimir Effect* (Oxford Univ. Press, 2009). ISBN: 978-0199238743
5. S. M. Carr, S. I. Woods, T. M. Jung, A. C. Carter, and R. U. Datla, “Experimental measurements and noise analysis of a cryogenic radiometer,” *Rev. Sci. Instrum.* **85**, 075105 (2014). doi:10.1063/1.4883191
6. H. B. Callen and T. A. Welton, “Irreversibility and Generalized Noise,” *Phys. Rev.* **83**, 34–40 (1951). doi:10.1103/PhysRev.83.34
7. E. Calloni, L. Di Fiore, G. Esposito, and L. Rosa, “Gravitational experiments in a quantum vacuum,” *Phys. Rev. D* **91**, 102002 (2015). doi:10.1103/PhysRevD.91.102002
8. H. B. G. Casimir, “On the attraction between two perfectly conducting plates,” *Proc. K. Ned. Akad. Wet.* **51**, 793 (1948).
9. C. S. Chang, S. G. Parker, and R. L. Byer, “Cryogenic optical resonators with 10^{-15} fractional frequency stability,” *Rev. Sci. Instrum.* **90**, 065112 (2019).
10. R. S. Decca, D. López, E. Fischbach, and D. E. Krause, “Measurement of the Casimir force between dissimilar metals,” *Phys. Rev. Lett.* **94**, 240401 (2005). doi:10.1103/PhysRevLett.94.240401
11. D. J. Fixsen, “The Temperature of the Cosmic Microwave Background,” *Astrophys. J.* **707**, 916–920 (2009). doi:10.1088/0004-637X/707/2/916

12. J. D. Jackson, *Classical Electrodynamics*, 3rd ed. (Wiley, 1999).
13. R. L. Jaffe, "The Casimir effect and the quantum vacuum," *Phys. Rev. D* **72**, 021301(R) (2005). doi:10.1103/PhysRevD.72.021301
14. A. J. H. Kamminga, "Vacuum Density and Cosmic Expansion: A QEV Model," *Preprints* (2025). doi:10.20944/preprints202509.0972.v1
15. A. J. H. Kamminga, "Vacuum Energy with Natural Bounds: A Spectral Approach without Fine-Tuning," *Preprints* (2025). doi:10.20944/preprints202507.0199.v2
16. G. L. Klimchitskaya, U. Mohideen, and V. M. Mostepanenko, "The Casimir force between real materials: Experiment and theory," *Rev. Mod. Phys.* **81**, 1827–1885 (2009). doi:10.1103/RevModPhys.81.1827
17. R. Kubo, "Statistical-Mechanical Theory of Irreversible Processes," *J. Phys. Soc. Jpn.* **12**, 570 (1957). doi:10.1143/JPSJ.12.570
18. R. Kubo, "The fluctuation-dissipation theorem," *Rep. Prog. Phys.* **29**, 255 (1966).
19. L. D. Landau and E. M. Lifshitz, *Electrodynamics of Continuous Media*, 2nd ed. (Pergamon, Oxford, 1984).
20. S. K. Lamoreaux, "Demonstration of the Casimir Force in the 0.6 to 6 μm Range," *Phys. Rev. Lett.* **78**, 5–8 (1997). doi:10.1103/PhysRevLett.78.5
21. J. C. Mather, D. J. Fixsen, R. A. Shafer, C. Mosier, and D. T. Wilkinson, "Calibrator design for the COBE Far Infrared Absolute Spectrophotometer (FIRAS)," *Astrophys. J.* **512**, 511–520 (1999). doi:10.1086/306805
22. K. A. Milton, *The Casimir Effect: Physical Manifestations of Zero-Point Energy* (World Scientific, 2001).
23. K. A. Milton, "The Casimir effect: Recent controversies and progress," *J. Phys. A: Math. Gen.* **37**, R209–R277 (2004). doi:10.1088/0305-4470/37/38/R01
24. K. A. Milton, "Applications of the Casimir effect," *J. Phys. Conf. Ser.* **161**, 012001 (2011). doi:10.1088/1742-6596/161/1/012001
25. U. Mohideen and A. Roy, "Precision Measurement of the Casimir Force from 0.1 to 0.9 μm," *Phys. Rev. Lett.* **81**, 4549–4552 (1998). doi:10.1103/PhysRevLett.81.4549
26. V. M. Mostepanenko, "Status of modern Casimir force measurements and theoretical approaches," *Universe* **7**, 84 (2021). doi:10.3390/universe7030084
27. B. A. Nosek *et al.*, "Promoting an open research culture," *Science* **348**, 1422–1425 (2015).
28. R. D. Peng, "Reproducible research in computational science," *Science* **334**, 1226–1227 (2011). doi:10.1126/science.1213847
29. Planck Collaboration, "Planck 2018 results. I. Overview and the cosmological legacy of Planck," *Astron. Astrophys.* **641**, A1 (2020). doi:10.1051/0004-6361/201833880
30. M. Rossi, D. Mason, J. Chen, Y. Tsaturyan, and A. Schliesser, "Measurement-based quantum control of mechanical motion," *Nature* **563**(7729), 53–58 (2018). doi:10.1038/s41586-018-0643-8
31. S. G. Kaplan, S. I. Woods, E. L. Shirley, A. C. Carter, T. M. Jung, J. E. Proctor, D. R. Sears, and J. Zeng, "Design, calibration, and application of a cryogenic low-background infrared radiometer for spectral irradiance and radiance measurements from 4 to 20 μm wavelength," *Opt. Eng.* **60**(3), 034102 (2021). doi:10.1117/1.OE.60.3.034102
32. A. Stange, M. Wagner, and F. M. de Leonardis, "Casimir force measurements in the deep submicron regime with optomechanical sensors," *Nat. Phys.* **18**, 271–276 (2022).
33. R. Steiner, "The new definition of the kilogram," *Metrologia* **54**, A1–A10 (2017).
34. V. Stodden, M. McNutt, D. H. Bailey *et al.*, "Enhancing reproducibility for computational methods," *Science* **354**, 1240–1241 (2016).
35. D. V. Strekalov, N. Yu, and C. M. Savory, "High-Q millimetre-wave whispering-gallery-mode resonators for frequency metrology," *IEEE Trans. Ultrason. Ferroelectr. Freq. Control* **68**(7), 2130–2140 (2021).
36. B. Taschuk and G. Wilson, "Good enough practices in scientific computing," *PLoS Comput. Biol.* **13**, e1005510 (2017). doi:10.1371/journal.pcbi.1005510
37. M. Urban, F. Couchot, X. Sarazin, and A. Lambrecht, "The quantum vacuum as the origin of the speed of light," *Eur. Phys. J. D* **67**, 58 (2013).